Systematic experimental and theoretical investigation of intersubband absorption in GaN/AlN quantum wells

M. Tchernycheva,* L. Nevou, L. Doyennette, F. H. Julien, and E. Warde
Action OptoGaN, Institut d'Electronique Fondamentale, Université Paris-Sud, UMR 8622 CNRS, 91405 Orsay cedex, France

F. Guillot, E. Monroy, and E. Bellet-Amalric
Equipe Mixte CEA-CNRS-UJF Nanophysique et Semiconducteurs, DRFMC/SP2M/PSC, CEA-Grenoble, 17 rue des Martyrs, 38054 Grenoble cedex 9, France

T. Remmele and M. Albrecht
Institut für Kristallzüchtung, Max-Born-Strasse 2, D-12489 Berlin, Germany
(Received 20 December 2005; revised manuscript received 13 February 2006; published 30 March 2006)

We have studied the electronic confinement in hexagonal (0001) GaN/AlN multiple quantum wells by means of structural (high-resolution x-ray diffraction and transmission electron microscopy) as well as optical characterizations, namely intersubband absorption and interband photoluminescence spectroscopies. Intense intersubband absorptions covering the 1.33–1.91 μm wavelength range have been measured on a series of samples with well thicknesses varying from 1 to 2.5 nm. The absorption line shape exhibits either a pure Lorentzian shape or multiple peaks. In the first case the broadening is homogeneous with a state-of-the-art low value of 67 meV. We deduce a dephasing time of the electrons in the excited subband T_2 of about 20 fs. For structured spectra the absorption can be perfectly reproduced with a sum of several Lorentzian curves; the individual peaks originate from absorption in quantum well regions with thickness equal to an integer number of monolayers. We have also carried out simulations of the electronic structure which point out the relevance of the nonparabolicity and many-body corrections on the intersubband absorption energy. The intersubband absorption exhibits a blue shift with doping as a result of many-body effects dominated by the exchange interaction. An excellent agreement with the experimental data is demonstrated. The best fit is achieved using a conduction band offset at the GaN/AlN heterointerfaces of 1.7±0.05 eV and a polarization discontinuity $\Delta P/(\epsilon_0\epsilon_r)$ of 10±1 MV/cm.

DOI: 10.1103/PhysRevB.73.125347 PACS number(s): 78.67.De, 81.07.St, 73.21.Fg

I. INTRODUCTION

III-nitride semiconductors are today intensively studied due to their appealing electronic and optoelectronic applications. Most of the optoelectronics applications, such as, for example, blue-ultraviolet light emitting diodes and laser diodes,[1,2] make use of the wide band gap of nitride semiconductors. Nitride heterostructures in the form of quantum wells or quantum dots are also promising candidates for high-speed intersubband (ISB) optical devices relying on the quantum confinement of electrons.[3] Room-temperature ISB absorptions have been reported by several groups in highly doped GaN/Al(Ga)N quantum wells (QWs) grown by molecular beam epitaxy[4–7] or metal organic chemical vapor deposition[8,9] and in GaN/AlN quantum dots.[10,11] The high conduction band offset of GaN/AlN heterostructures (~1.75 eV) allows tailoring ISB transitions to wavelengths as short as 1.08 μm.[6] Nitride heterostructures are good candidates for ISB devices operating in the near infrared spectral range and, in particular, at fiber-optics telecommunication wavelengths. Nitride QWs also show ultrafast ISB carrier dynamics due to a strong Fröhlich interaction in these highly ionic materials.[3] The ISB absorption recovery time has been measured to be in the 140–400 fs range,[12–14] which is significantly shorter than the corresponding time measured in GaAs QWs. This offers prospects for the development of ultrafast ISB devices such as optical switches operating at Tbit/s data rate.

Because of the rather large effective mass of electrons in GaN ($m_0 \sim 0.22m_0$, where m_0 is the free electron mass), very thin QW layers, typically 4–6 monolayers (1–1.5 nm) are required in order to tune the ISB absorption in the 1.3–1.55 μm wavelength domain. For such thin QWs the ISB transition energy is extremely sensitive to the QW width, therefore it is crucial to fabricate structures with abrupt interfaces and to control the layer thicknesses down to 1 monolayer (1 ML for bulk GaN equals to 0.25928 nm). This represents a major challenge for the epitaxial growth.

It is well known that the optical properties of nitride QWs are strongly affected by the presence of an internal electric field.[15] This field, inherent to the wurtzite-phase nitride heterostructure grown along the c axis, arises from the piezoelectric and spontaneous polarization discontinuity between the well and barrier materials. The built-in field can be extremely strong [about 8–10 MV/cm for isolated GaN/AlN QWs (Refs. 7 and 16)]. Modeling of quantum confinement in nitride QWs should therefore go beyond the flat-band approximation and account for the internal electric field in the QW and in the barriers. For the QWs wider than 7 ML (1.8 nm) the electric field has a major effect on the ISB transition energy.[6] The internal field value is often introduced into the calculation as an adjustable parameter.[12,18]

Most of the calculations of the ISB transitions make use of the effective mass model restricted to the conduction band (CB),[6,12,18,19] but except in Ref. 19 the CB nonparabolicity is

 ©2006 The American Physical Society

usually neglected. Indeed, one would expect the nonparabolicity corrections to be weak because of the wide band gap of GaN. However for thin GaN/AlN QWs exhibiting an ISB transition at telecommunication wavelengths, the energy of the excited state is so large that it is strongly affected by the nonparabolicity, as will be shown in this paper. Other usually ignored corrections stem from the large electron concentration in the $10^{19}-10^{20}$ cm^{-3} range,[4–7,20] which is required for observing ISB absorption in GaN/AlN QWs. At these concentrations, the screening of the internal electric field and the many-body interactions become important. Up to now, not enough attention has been paid to these issues.

The CB discontinuity at the GaN/AlN interface is also a critical parameter which strongly influences short-wavelength ISB transitions. The values reported in the literature based on photoemission experiments cover the range from 1.4 eV (Ref. 21) up to 2.65 eV.[22] Early studies of electron confinement in GaN/AlN QWs assumed a CB offset equal to 2 eV.[3,6,20]

In this paper we present a systematic experimental and theoretical study of ISB transitions of hexagonal-phase GaN/AlN multiple quantum wells grown alone (0001) direction with well thicknesses ranging from 4 to 10 ML. The study provides a detailed understanding of the electronic confinement in these ultrathin layers. Intense ISB absorptions are observed in the wavelength range of 1.33–1.91 μm and the ISB broadening is as low as 67 meV, which corresponds to the state-of-the-art of nitride heterostructure epitaxial growth. We show that the absorption spectrum is the sum of Lorentzian-shaped absorptions peaked at energies corresponding to well thicknesses equal to an integer number of monolayers. The quantum confinement is modeled using the envelope function approximation restricted to the CB. To account for the CB nonparabolicity, the energy dependence of the effective mass is introduced based on the eight band $\mathbf{k}\cdot\mathbf{p}$ dispersion relation for bulk GaN. We show that for thin QWs the nonparabolicity has a major effect on the ISB absorption energy. The doping-related effects are included via the self-consistent solution of the Schrödinger-Poisson equations with the subsequent application of the many-body corrections. The results of the simulation of both the ISB absorption energy and the photoluminescence energy are then compared with measurements. This allows to independently refine the value of two material parameters, namely, the polarization discontinuity and the CB offset at the GaN/AlN interfaces. In particular, the best fit with experimental results is obtained for a CB offset of 1.65–1.75 eV, which is significantly lower than the previously accepted value of ~2 eV.

II. EXPERIMENTAL ASPECTS

A. Sample fabrication

We have investigated a set of 21 samples containing GaN/AlN multiple quantum well (MQW) structures grown by plasma-assisted molecular-beam epitaxy on *c*-sapphire substrates with an AlN buffer layer. Samples consist of 20 periods of GaN QWs with 3-nm-thick AlN barriers, sandwiched between two Si-doped GaN claddings. The doping level of the claddings was in the 10^{18} cm^{-3} range and their thickness varies between 100–600 nm for the lower cladding and 10–100 nm for the top cladding. The MQW sample parameters are summarized in Table I. The first six samples (GS1-GS6) are unintentionally doped (UD), while for all other samples, silicon was incorporated into the QWs at a concentration of 5×10^{19} cm^{-3}, in order to provide an electron population of the ground state.

All the layers are grown under metal rich conditions, as required to achieve two-dimensional growth of III-nitrides by plasma assisted molecular beam epitaxy. Three different growth procedures were used for the MQW region, namely procedures using growth interruptions, Ga as a surfactant, or using In as a surfactant. Based on the optical microscopy measurements none of the samples present cracks on the surface, independent of the growth procedure. The root mean square surface roughness measured by atomic force microscopy remained always around 1 nm, measured over a surface of 5×5 μm^2.

Using the growth interruption (GI) technique, samples are grown at 720 °C, the AlN barriers are grown under Al-rich conditions, and GaN QWs are grown under Ga-rich conditions. After the growth of each AlN barrier, a growth interruption under nitrogen flux is required to consume the Al excess accumulated on the surface. In contrast, after the growth of each GaN QW it is not necessary to introduce a second growth interruption, since the Ga excess segregates on the AlN and is rapidly desorbed at this substrate temperature. (These samples are referred to as GI1-GI3 in Table I.)

An alternative approach to achieve two-dimensional AlN barriers consists on using Ga as a surfactant for the growth of AlN, with the Al flux corresponding to the Al/N stoichiometry and using an additional Ga flux to stabilize the surface. This Ga excess segregates on the surface and it is not incorporated into the AlN layer. Since Ga is used as a surfactant both for the GaN QWs and for the AlN barriers, no growth interruptions are required along the complete structure. Sharp GaN/AlN interfaces have been demonstrated by using this growth procedure.[23] (These samples are referred to as GS1-GS17 in Table I.)

Another possibility to achieve two-dimensional heterostructures is to perform the growth of GaN QWs and AlN barriers using the Ga and Al fluxes corresponding to the Ga/N and Al/N stoichiometry, and to provide the metal excess by introducing an additional In flux.[24] In this case, it is necessary to reduce the substrate temperature to around 680 °C, low enough to guarantee a good In coverage and high enough to prevent In incorporation. The In flux has been tuned to stabilize an In coverage of 1 ML segregating at the growth front. (This procedure was used for fabrication of the IS1 sample.)

B. Structural characterizations

The desorption of Ga and GaN during the QW growth and AlN overgrowth is known to have an effect on the QW thickness.[25] In order to obtain the precise QW thickness, the period of the MQW structures and average Al content have been determined by high-resolution x-ray diffraction

TABLE I. Sample parameters. The labels "GS," "IS," and "GI," respectively, stand for growth procedures with Ga as a surfactant, In as a surfactant, and growth interruptions. Doping level in the QWs. QW thickness [superscripts TEM (XR) stand for QW thickness deduced from TEM (HRXRD) measurements, if not stated otherwise the nominal value is given], e_{12} and e_{13} ISB absorption energies and the PL energy with the corresponding broadening in eV.

Sample ref.	Doping (cm^{-3})	QW thickness (nm)	e_{12} (FWHM) (eV)	e_{13} (FWHM) (eV)	PL energy (FWHM) (eV)
GS1	UD	0.8 ± 0.26^{XR}	0.895(0.095)		3.91(0.12)
GS2	UD	0.8 ± 0.26^{XR}	0.88(0.1)		3.717(0.135)
GS3	UD	1.3	0.854(0.104)		3.757(0.375)
GS4	UD	1.5	0.78(0.14)		3.454(0.316)
GS5	UD	1.8 ± 0.26^{XR}	0.685(0.105)	1.2(0.126)	3.258(0.117)
GS6	UD	2.5	0.64(0.068)	1.198(0.178)	3.153(0.192)
GS7	5×10^{19}	1	0.927(0.099)		3.963(0.137)
GS8	5×10^{19}	1	0.932(0.101)		3.977(0.158)
GS9	5×10^{19}	0.8 ± 0.26^{XR}; $0.78-1.04^{TEM}$	0.903(0.092)		3.91(0.14)
GS10	5×10^{19}	1.3	0.866(0.105)		3.703(0.13)
GS11	5×10^{19}	1.3	0.881(0.159)		3.716(0.16)
GS12	5×10^{19}	1.3	0.851(0.175)		3.772(0.135)
GS13	5×10^{19}	1.45 ± 0.26^{XR}	0.874(0.138)		3.607(0.17)
GS14	5×10^{19}	$1.04-1.3^{TEM}$	0.866(0.067)		3.691(0.13)
GS15	5×10^{19}	1.5	0.8(0.133)		3.55(0.124)
GS16	5×10^{19}	1.65 ± 0.26^{XR}	0.729(0.134)		3.69(0.24)
GS17	5×10^{19}	2.05 ± 0.26^{XR}	0.689(0.14)	1.198(0.172)	3.37(0.17)
IS1	5×10^{19}	1.25 ± 0.26^{XR}; $1.04-1.3^{TEM}$	0.875(0.14)		3.64(0.2)
GI1	5×10^{19}	1.8 ± 0.26^{XR}	0.7(0.123)	1.25(0.115)	3.4(0.5)
GI2	5×10^{19}	2.05 ± 0.26^{XR}; $2.08-2.6^{TEM}$	0.665(0.112)	1.2(0.144)	3.336(0.455)
GI3	5×10^{19}	2.35 ± 0.26^{XR}	0.649(0.08)	1.156(0.147)	3.281(0.5)

(HRXRD) measurements using a SEIFERT XRD 3003 PTS-HR diffractometer with a beam concentrator prior to the Ge(220) four-bounce monochromator and a Ge(220) two-bounce analyzer in front of the detector. Figure 1 displays the $2\theta-\theta$ scan of the (0002) reflection of some MQW samples. The peaks labeled "GaN" and "AlN" correspond to the reflection from the GaN claddings and AlN buffer layer, respectively. The observation of several satellites of the superlattice reflection (labeled SL) is an indication of the good quality of the interfaces. The diffraction angle of SL peak provides information on the mean lattice parameter along the c axis of the MQWs and the intersatellite angle gives a measurement of the superlattice period. Analyses of the reciprocal space map on the (−1015) reflection on several MQWs reveal that GaN is under compressive strain of 40–45 % on the AlN. [The strain state of a layer is defined as $100\times(1-(a_m-a_S)/(a_0-a_S))$, where a_m, a_S and a_0 are the in-plane lattice parameter of the measured layer, of the substrate and of the fully-relaxed layer, respectively.]

X-ray diffraction provides the mean superlattice period with a high precision, better than 0.1 nm.[26] However it does not take into account thickness fluctuations and does not directly provide the thickness of the barrier and the well. The QW and barrier thicknesses were calculated with an accuracy

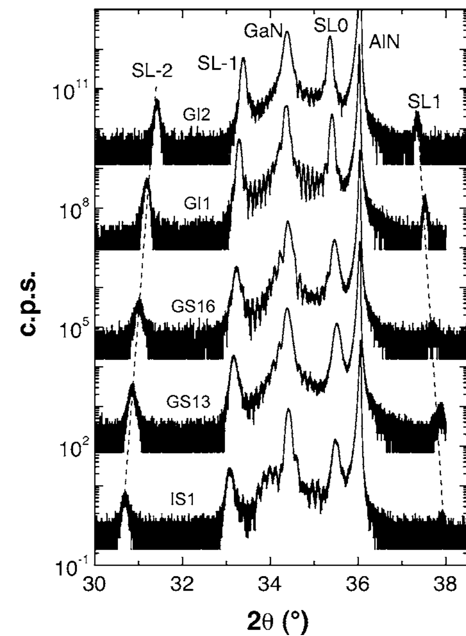

FIG. 1. $2\theta-\theta$ scan of the (0002) reflection of GaN/AlN MQW structures.

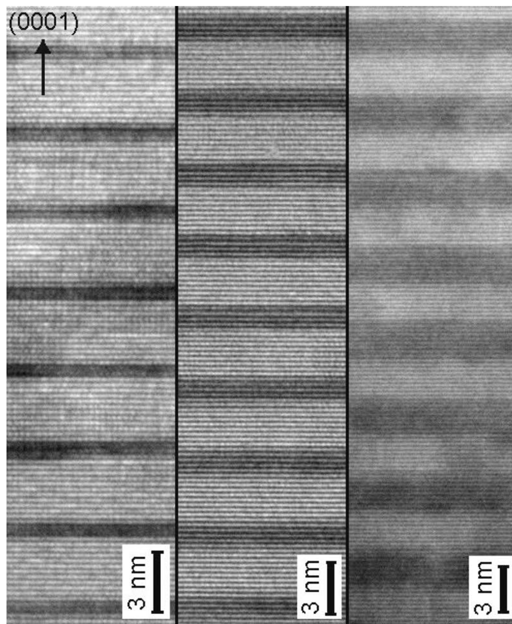

FIG. 2. From left to right: high resolution TEM images of GS9, IS1, and GI2 samples grown using Ga as a surfactant, In as a surfactant and growth interruption techniques, respectively. Dark (bright) regions correspond to GaN (AlN). Growth axis is directed upwards.

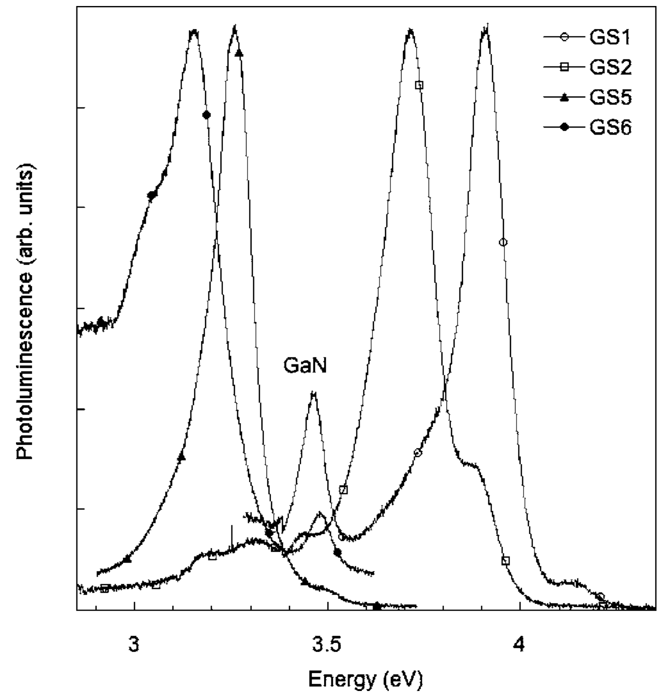

FIG. 3. Room-temperature PL spectra of undoped samples grown using Ga as surfactant.

of ±1 ML. The found barrier thickness is about 2.8±0.52 nm for all the samples and the QW thicknesses are reported in Table I.

Further analyses of the QW thickness and interface roughness were performed by means of high-resolution transmission electron microscopy (HRTEM) on three samples fabricated using Ga as surfactant (GS9), In as surfactant (IS1), and performing growth interruption (GI2). The hexagonal wurtzite structure of GaN/AlN has a chemical sensitive (000±2) reflection, which can be used to easily distinguish between GaN and AlN by image intensity. HRTEM images are taken with the sample tilted approximately 5° out of the zone axes around the [0001] growth direction. In this so-called three beam case mainly the (000±2) and (0000) reflections contribute to the interference pattern revealing the (0002) lattice fringes. Tilting out of the zone axes reduces the number of reflections forming the image leading to a simple pattern that is not as sensitive to local strain and sample thickness variation as in the zone axes orientation.

Figure 2 displays the HRTEM images of MQWs in GS9, IS1, and GI2 samples. Dark (bright) regions in the images correspond to GaN (AlN). The in-plane thickness fluctuations of ±1 ML on a length scale of 10–20 nm have been observed.

The layer thicknesses deduced from HRTEM measurements are summarized in Table I. The uncertainty in the measured values corresponds to the ML thickness fluctuations. As seen for samples GS9, IS1, and GI2, the thickness values deduced separately from HRTEM and HRXRD are in good agreement. It should be noted that HRXRD gives the QW thickness averaged in the layer plane over the area corresponding to the spot size (around 20 mm^2), while HRTEM provides a local measurement allowing estimating thickness fluctuations on the nanometer scale. As will be shown below, both measurements are in good agreement with QW thicknesses deduced from optical measurements.

C. Optical spectroscopic measurements

The fundamental interband transition in MQW samples was probed by means of photoluminescence (PL) spectroscopy at room temperature. The ultraviolet excitation at $\lambda = 244$ nm was provided by a frequency-doubled continuous-wave Ar laser and the luminescence was collected by a 0.46 m focal length spectrometer equipped with a charge-coupled device camera. The PL peak energy and full width at half maximum (FWHM) are indicated in Table I for all investigated samples.

Figure 3 shows the PL spectra of four undoped samples, containing QWs with thicknesses varying from 4 to 10 ML (1–2.5 nm). As expected, the PL peak energy is redshifted when increasing the QW thickness because of the quantum confined Stark effect induced by the internal electric field. For QWs thicker than 7 ML (1.8 nm) the PL energy is smaller than the band gap of bulk GaN and is extremely sensitive to the actual value of the internal field.

The PL measurements also provide some information on the sample homogeneity. The broadening of the PL signal for samples grown with Ga or In as surfactant is in the 0.12–0.24 eV range. However, for GI1–GI3 samples fabricated with growth interruptions, the FWHM is strongly increased up to 0.5 eV which could be the consequence of local fluctuations of either thickness or electric field.

For almost all samples, a peak at 3.46–3.48 eV is observed originating from the GaN cladding layers. The PL

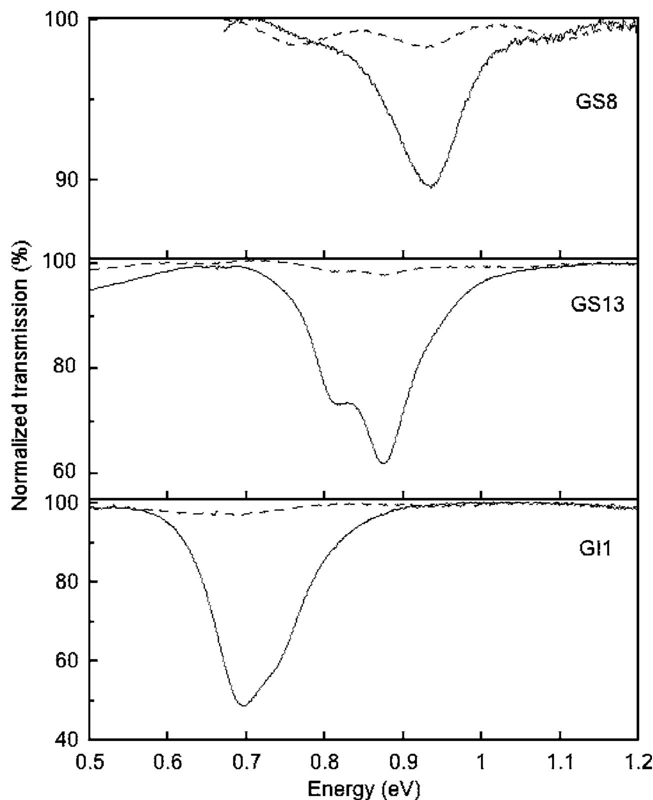

FIG. 4. Room-temperature transmission spectra of GS8, GS13, and GI1 samples for *p*-polarized (solid lines) and *s*-polarized (dashed lines) light. The QW thicknesses are equal to 4, 5, and 7 ML, respectively. Spectra are normalized to 100% in the high-energy region where no absorption is observed.

energy is shifted with respect to the 3.39 eV value of the GaN bulk band gap at room temperature. This is probably a consequence of the compressive strain of the claddings (and the entire structure) because of the underlying AlN buffer layer.

The ISB absorption of the samples was investigated using Fourier transform infrared spectroscopy. The sample facets were polished at 45° angle to form a multipass waveguide with 4–6 total internal reflections. The transmission for *p*- and *s*-polarized light was measured at room temperature using a deuterated triglycine sulfate photodetector. All samples show a pronounced *p*-polarized absorption peaked in the 1.33 to 1.91 μm wavelength range. No absorption was found for *s*-polarized light within experimental accuracy. The transmission spectra for *s*-polarization only exhibit periodic oscillations arising from the interferences in the AlN buffer and the epitaxial layers. The *p*-polarization of the absorption is a signature of an ISB transition between electron states confined in the QW.[27] As an example, Fig. 4 shows the transmission spectra of GS8, GS13, and GI1 samples for *p* (full curves) and *s* (dashed curves) light polarizations. The *p*-polarized absorption resonances shift to lower energies when increasing the QW thickness. As seen, for thin (4–6 ML) QWs the ISB absorption covers the telecommunication wavelength range. The ISB absorption efficiency is high: for GI1 sample it attains 52%, which corresponds to 8.6% per one internal reflection in the multipass waveguide. The ISB peak energies along with the corresponding FWHM are reported in Table I.

IR transmission measurements performed on nominally undoped samples also reveal ISB absorptions, thus indicating that the ground subband of the QWs is populated with electrons. This unexpected finding cannot be explained by the GaN residual doping, which is estimated from separate Hall measurements to be of the order of 10^{17} cm^{-3}. The latter value is too weak to provide a detectable ISB absorption. The residual electron population may originate from surface donor states. Indeed, it has been pointed out that in the GaN/AlGaN field effect transistors the surface donors are responsible for the formation of the two-dimensional electron gas at the heterointerface.[28] However for MQW samples the surface states are unlikely to be the only carrier source. Deep donor states in the AlN barriers should have a major contribution. Indeed, another possible mechanism of the fundamental subband filling is the ionization of the defect states in the AlN barriers. It is well known that oxygen, for example, is a common substitutional impurity, which can be present in large concentrations in AlN. The incorporation of oxygen in AlN leads to a deep-defect band with a broad energy range $\sim$0.7– $\sim$2.7 eV below the conduction band of AlN.[29] It is expected that the deep levels with an energy higher than that of the ground state of the QW will contribute to populate the ground state, giving rise to the residual absorption.

Figures 5(a) and 5(b) show the *p*-polarized absorbance spectrum of the GS series samples. As already mentioned, the energy of the ISB absorption is blue-shifted when the well thickness is reduced. Examining the ISB absorbance lineshape for the whole series of samples is quite informative. Indeed, two different behaviors are observed: the absorbance resonance either exhibits a purely Lorentzian lineshape or is structured with two or three well-defined peaks. Figure 5(c) shows the absorbance spectrum (full line) and the corresponding Lorentzian fit (dashed line) for the GS14 sample. The absorbance spectrum is perfectly fitted with a Lorentzian curve with a FWHM of 67 meV. This remarkably small value corresponds to the state-of-the-art for GaN/AlN QWs grown by molecular beam epitaxy.[6] A Lorentzian lineshape can only be attributed to a homogeneously broadened resonance. The FWHM is related to the dephasing time of electrons in the excited subband, which has been shown to be dominated by the electron-electron scattering processes.[3] The T_2 dephasing time can be estimated as $T_2=\frac{2\hbar}{\Delta E}=19.6$ fs—in good agreement with the value of $\sim$10 fs calculated in Ref. 3

The sample GS15 shows a good example of structured ISB absorbance line shape. As seen in Fig. 5(d), its absorbance spectrum exhibits three peaks separated by 63 and 57 meV, respectively. The multiple peaks cannot be explained by Fabry-Perot oscillations arising from interferences in the active and buffer layers because these oscillations, which are observed under *s* polarization, have a period of about 150 meV for this sample. The absorbance line shape (full line) is perfectly fitted with a sum of three Lorentzian resonances (dashed lines) with a FWHM $\sim$40 meV. For all other samples with structured absorbance spectrum, we also find a good fit with a sum of two or three Lorentzian curves with similar broadening. One likely interpretation for the

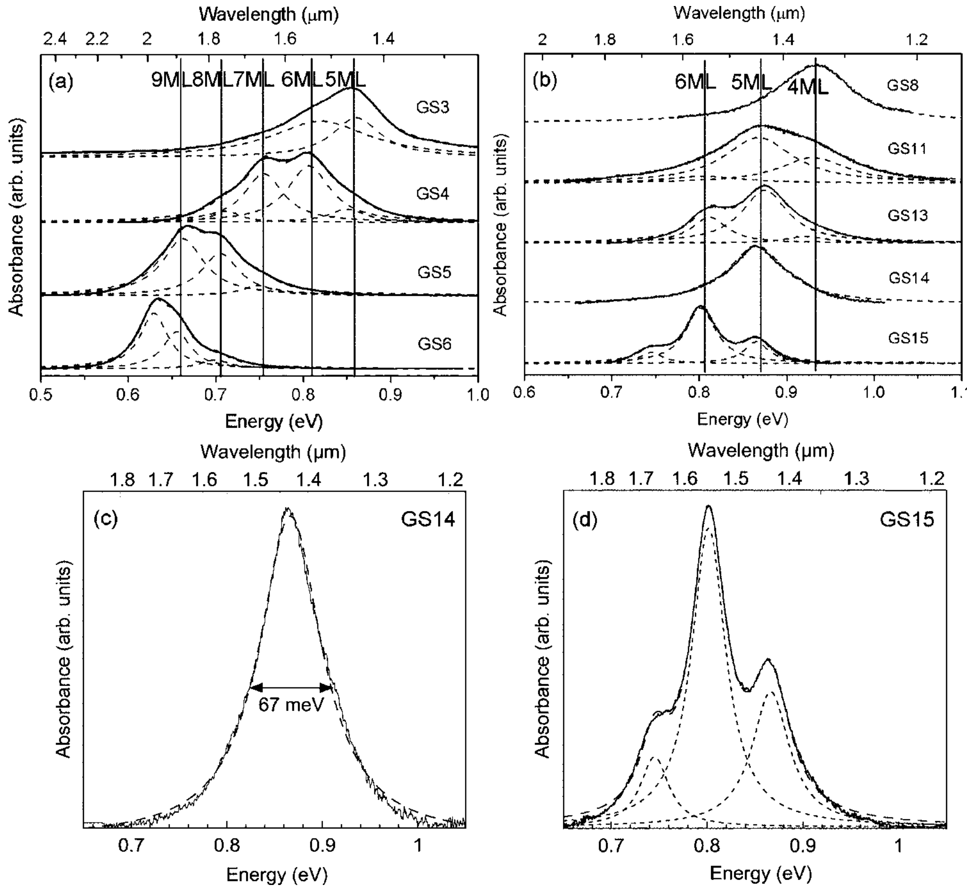

FIG. 5. Absorbance spectra of nominally undoped (a) and doped (b) samples, vertical lines mark the mean energies of structures. The curves are vertically shifted for clarity. (c) Absorbance of GS14 sample (full line) and the corresponding Lorentzian fit (dashed line). (d) Absorbance of GS15 sample (full line), Lorentzian fitting curves (dotted lines), and sum of Lorentzian fits (dashed line).

multiple peaks is that these peaks originate from absorbance in QW regions with different thicknesses. This effect has already been mentioned in Refs. 12 and 19 to explain the shoulders in ISB absorption spectra. However, in contrast to previously reported results, in this sample the broadening of the individual peaks is small enough to observe the multiple peaks so clearly resolved.

Thickness fluctuations of the order of 1 ML can originate from variation of the growth rate with time (fluctuations of the mean QW thickness from period to period in the superlattice), or from in-plane inhomogeneities. Since a low growth rate of 0.3 ML/s has been chosen for the sample fabrication, the fluctuations of the mean QW thickness should be smaller than 1 ML. Therefore, the most likely explanation of the ISB absorption shape is the presence of in-plane thickness fluctuations in the QWs.

One major result is that the peaks in the absorbance spectra occur at almost the same energy in the various samples within a standard deviation of less than 15 meV. The discrete peak energies, pointed by vertical bars in Figs. 5(a) and 5(b), correspond to the ISB resonance of QW regions with a thickness equal to an integer number of MLs. It should be noted that for ultrathin GaN QWs considered in this study, a 1 ML increase of the thickness translates into a strong ISB energy shift, of about 60 meV for 4–5 ML-thick QWs. This value is comparable to the broadening factor, and therefore results in structuring of the absorbance spectrum instead of the inhomogeneous broadening. As a comparison, in material systems such as GaAs/AlGaAs or InGaAs/InAlAs, the minimal thickness necessary to have two bound levels in the well is much larger than in the GaN/AlN system, of the order of several nanometers. For such large thicknesses a fluctuation of 1 ML only results in a small shift of the ISB absorption energy. If the lateral length scale of the fluctuations is bigger than the Fermi wavelength of the electrons, the fluctuations manifest in the ISB spectra as an inhomogeneous broadening, otherwise they contribute to the homogeneous broadening.[17]

The integer numbers of MLs corresponding to the discrete peaks are shown in Figs. 5(a) and 5(b). The values are in agreement with the thickness deduced from HRTEM or HRXRD measurements.

For the thicker QW samples a weak *p*-polarized absorption is observed at high energy in addition to the main absorption. Figure 6 shows the absorbance spectrum of GI3 sample where the high-energy resonance is clearly observed at 1.16 eV with an amplitude 20 times smaller than that of the main peak and a large FWHM of 147 meV. We attribute the high-energy absorption to the transition from the ground subband e_1 to the third subband e_3 in agreement with previous observations by Hoshino *et al.*[18] This transition is allowed in nitride QWs because of the presence of strong internal electric field in the well that breaks the symmetry of the potential.

III. MODELING OF THE ELECTRON QUANTUM CONFINEMENT IN GAN/ALN QUANTUM WELLS

The first step of the simulations is to calculate the conduction band profile and to account for the band bending

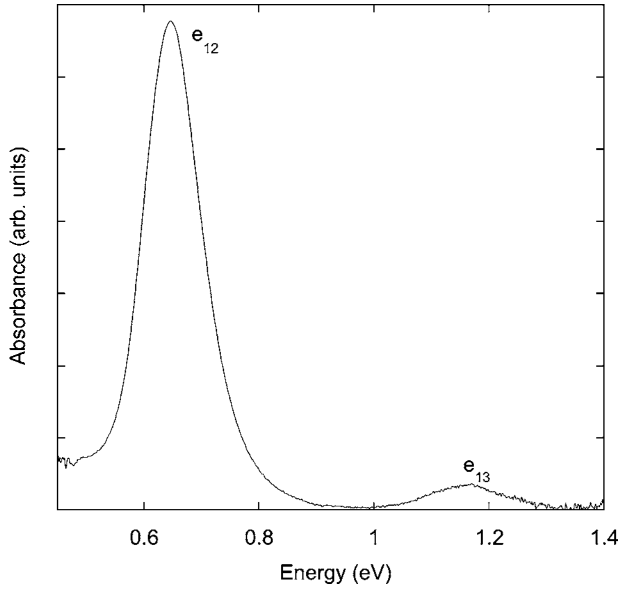

FIG. 6. ISB absorbance of GI3 sample. Two peaks are observed, attributed to the e_{12} and e_{13} transitions.

across the active multiple quantum wells. The model uses the semi-classical Thomas-Fermi approximation.[30] Figure 7 shows the CB profile calculated for a 10 period active structure between two GaN layers n-doped at 10^{18} cm^{-3}. The QWs are 1.3 nm thick and doped at 5×10^{19} cm^{-3}. Two domains can be found within the active region: a high-field domain closer to the surface where the potential drop is large and a low-field domain where the potential drop over one period is almost zero. The two QWs in the high-field domain are above the Fermi level. Consequently they should be depleted and do not participate in the ISB absorption. For QWs within the low-field domain the bandstructure is periodic,

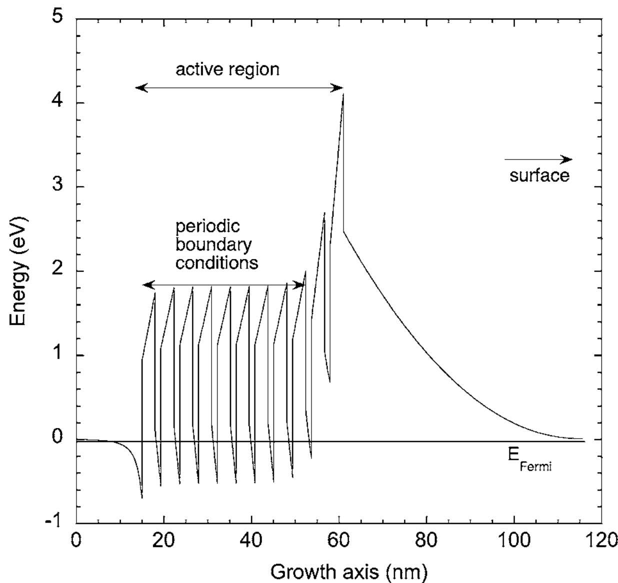

FIG. 7. CB potential profile calculated using Thomas-Fermi approximation for 10 periods of 1.3 nm thick GaN QWs doped at 5×10^{19} cm^{-3} with 3 nm thick AlN barriers sandwiched between two thick GaN layers doped at 10^{18} cm^{-3}.

thus the internal electric field in the well F_w and in the barriers F_b can be calculated according to[31,32]

$$F_w = -\frac{\Delta P}{\epsilon_0}\frac{L_b}{L_b\epsilon_w + L_w\epsilon_b},$$

$$F_b = \frac{\Delta P}{\epsilon_0}\frac{L_w}{L_b\epsilon_w + L_w\epsilon_b}, \qquad (1)$$

where ΔP is the polarization discontinuity between GaN and AlN, L_b (L_w) is the barrier (well) thickness, and ϵ_b (ϵ_w) stands for the static dielectric constant of AlN (GaN).

Hereafter, we will only consider the populated QWs in the low-field domain and we will assume a zero potential drop over one period. The electronic confinement for one period is calculated within the envelope function approximation restricted to the CB. The Schrödinger equation is solved using the transfer-matrix method.[33] In order to account for the CB nonparabolicity, we consider an energy dependent effective mass. The dispersion relation along the c axis for bulk GaN $E(k_z)$ is calculated using the eight-band $\mathbf{k}\cdot\mathbf{p}$ model accounting for strain.[34] The energy dependent effective mass is then defined by $m^*(E)=\frac{\hbar^2k_z^2}{2E(k_z)}$. For the calculations we use a quadratic polynomial fit of the energy dependent effective mass of GaN

$$m^*(E) = 0.22m_0(1 + 0.613E + 0.057E^2),$$

where E is an energy in eV measured from the CB edge.

In order to illustrate the relevance of the nonparabolicity correction, Fig. 8 shows the energy dispersion of the CB of bulk GaN along the c axis calculated using an eight band $\mathbf{k}\times\mathbf{p}$ model along with the parabolic dispersion with an energy-independent effective mass $m^*=0.22m_0$. As seen in Fig. 8, the nonparabolic corrections becomes important for wave vectors $k_z>0.15$ Å^{-1}, i.e., for energies higher than 300 meV with respect to the CB minimum. For QWs absorbing at 1.3–1.55 μm, the correction due to the nonparabolicity cannot be neglected since the excited state lies at an energy 1.5 eV above the CB minimum. This is illustrated in the inset of Fig. 8 that shows the potential profile, energy levels and the corresponding envelope functions for 1.56 nm thick QW between 3 nm thick AlN barriers calculated assuming parabolic dispersion (dashed lines) and nonparabolic dispersion (full lines). The e_{12} energy is 0.983 eV in the parabolic case, and it is reduced to 0.727 eV by taking the nonparabolicity into account, i.e., the correction due to the CB nonparabolicity exceeds 25%.

As far as the AlN barrier is concerned, the effective mass is not perfectly known. However we have separately checked by numerical tests that its influence on the calculated energy levels is rather weak. We take a value of $0.31m_0$ independent on the energy.[35]

Since most of the investigated samples are populated with electrons at a large concentration, the model of one electron in an empty conduction band is no longer satisfactory. In particular, one should take into account the Coulomb interaction of electrons with ionized donors as well as between free carriers. In order to do this, we first calculate the energy levels and corresponding envelope function within the Har-

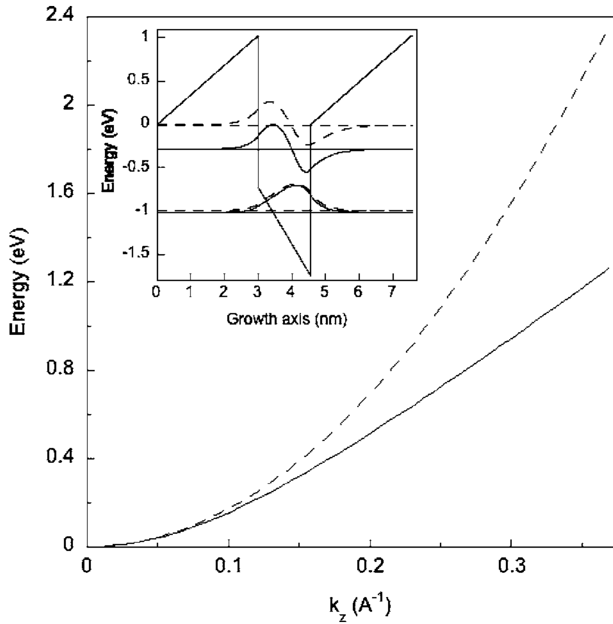

FIG. 8. Dispersion relation $E(k_z)$ calculated using the eight-band $\mathbf{k}\cdot\mathbf{p}$ model for bulk GaN (full line) and the parabolic dispersion with the effective mass $m^*=0.22m_0$. Inset: potential profile, energy levels and the corresponding envelope functions for 1.56 nm thick QW between 3 nm thick AlN barriers calculated assuming parabolic dispersion (dashed lines) and nonparabolic dispersion (full lines).

tree approximation by solving the Schrödinger and Poisson equations self-consistently. The iterative procedure starts with unperturbed potential profiles, i.e., constant electric fields in the well and barriers given by Eq. (1). The Schrödinger equation is then solved for that given potential and we calculate the Fermi energy and electron population of each energy state. We then solve the Poisson equation in order to calculate the corrections to the potential profile.[36] Iterations are repeated until the energy variation of all confined levels becomes inferior to 0.1 meV.

The Hartree correction gives rise to a screening of the internal electric field in the well by free carriers. Because the screened potential profile in the well tends to flatten, one expects a reduction of the ISB transition energy when increasing the carrier concentration, which is indeed predicted by the model. However, previously reported experimental measurements show just the opposite behavior: the ISB energy for doped samples is systematically blueshifted with respect to the UD samples.[7] This apparent contradiction can be clarified by taking into consideration the many-body interactions, namely, the electron-electron exchange interaction, the excitonic interaction and the depolarization shift.[7,37]

In the Hartree-Fock approximation the exchange interaction appears as an additional term in the Schrödinger equation.[38] This term has a nonlocal nature, which renders the exact solution very computationally intensive.[39] To avoid computational difficulties, it is possible to estimate the contribution of the exchange interaction using the perturbation theory. We have followed the approach proposed by Bandara *et al.*,[40] where Hartree envelope functions are used as a basis and the first perturbative correction of the energy is calculated. The authors show that the exchange interaction mainly affects the fundamental subband e_1 by lowering its energy, which results in an increase of the ISB transition energy. If one neglects the thermal excitation, the modification of the e_1 subband energy is given by

$$\Delta e_1^{\text{exch}} = -\frac{e^2}{2\epsilon_0\epsilon_r}\int_{-\infty}^{\infty} dz \int_{-\infty}^{\infty} dz' \int_0^{k_F} \frac{k'dk'}{2\pi}\frac{e^{-k'|z-z'|}}{k'} \times |\Psi_1(z')|^2|\Psi_1(z)|^2,$$

where ϵ_r is the dielectric constant of the QW material, the integration is carried out over the modulus of the in-plane wave vector k', k_F is the Fermi wave vector related to the surface carrier density n_S by $k_F=\sqrt{2\pi n_S}$ and Ψ_1 is the envelope function for the fundamental subband calculated within Hartree approximation.

The other many-body corrections, which become important at large carrier concentrations, are the depolarization shift α and the excitonic interaction β. The depolarization shift, which reflects the resonant screening of the external infrared field by the collective oscillation of the electron plasma, results in an increase of the transition energy, in contrast to the excitonic shift. The excitonic correction stems from the Coulomb interaction between the excited electron and the quasi-hole formed in the ground subband. The effective absorption energy of the electron gas e_{12}^{coll} is given by

$$e_{12}^{\text{coll}} = e_{12}\sqrt{1+\alpha-\beta},$$

where e_{12} is ISB transition energy for single electron transition.[41,42] Assuming only two subbands, the depolarization correction can be expressed as[41]

$$\alpha = \frac{2e^2 n_S}{\epsilon_0\epsilon_r e_{12}}\int_{-\infty}^{\infty} dz\left(\int_{-\infty}^{z} dz'\Psi_1(z')\Psi_2(z')\right)^2,$$

where ϵ_r is the high-frequency dielectric constant of GaN, n_S is the surface carrier density, and Ψ_1 and Ψ_2 are the envelope functions of the ground and first excited subband, respectively.

The excitonic correction can be estimated using[43]

$$\beta = -\frac{2n_S}{e_{12}}\int_{-\infty}^{\infty} dz|\Psi_1(z)|^2|\Psi_2(z)|^2\frac{\partial V_{\text{xc}}[n(z)]}{\partial n(z)},$$

where the exchange-correlation energy $V_{\text{xc}}[n(z)]$ is expressed as the following functional of the 3D carrier density $n(z)$:

$$V_{\text{xc}}[n(z)] = -\frac{2}{r_s}\left(\frac{9}{4\pi^2}\right)^{1/3}\frac{e^2}{8\pi\epsilon_0\epsilon_r a^*} \times\left[1+0.7734\frac{r_s}{21}\ln\left(1+\frac{21}{r_s}\right)\right],$$

with dimensionless parameter $r_s=\sqrt[3]{\frac{3}{4\pi(a^*)^3 n(z)}}$ and the effective Bohr radius $a^*=\frac{4\pi\epsilon_0\hbar^2}{m_0e^2}\frac{\epsilon_r}{m^*/m_0}$.

Figure 9 shows the e_{12} transition energy calculated for a 1.56 nm thick GaN QW with 3 nm thick AlN barrier as a function of the surface carrier density. The effect of each many-body correction is separately shown in order to com-

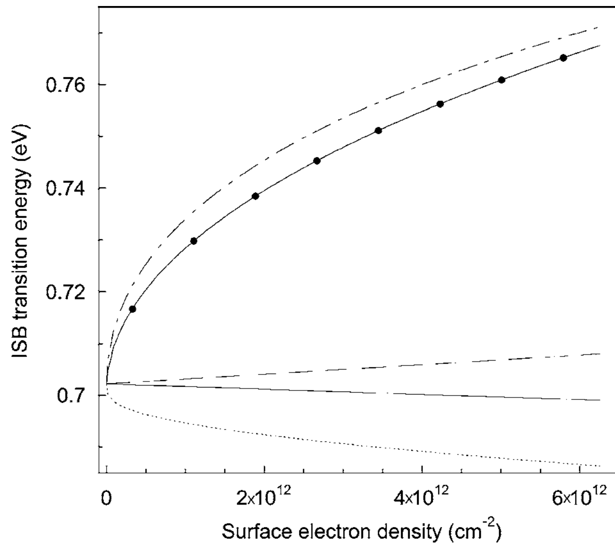

FIG. 9. ISB transition energy e_{12} as a function of surface electron density calculated in the Hartree approximation (full line), including separately exchange correction (dashed-dotted line), depolarization shift (dashed line) and excitonic shift (dotted line) and taking into account all many-body corrections (full line with black circles). Calculation was performed for 1.56 nm thick doped QW between 3 nm thick undoped barriers.

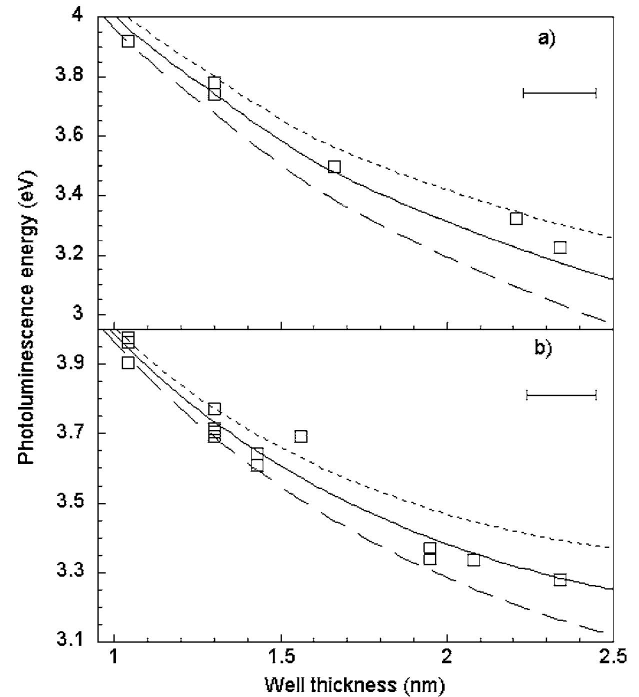

FIG. 10. Calculated PL energy for (a) UD and (b) doped samples as a function of QW thickness for $\frac{\Delta P}{\epsilon_0 \epsilon_r}$ equal to 8 MV/cm (dotted curves), 10 MV/cm (full curves), and 12 MV/cm (dashed curves). The horizontal bar equal to 1 ML shows the thickness uncertainty.

pare their relative importance. The full curve represents the e_{12} obtained from self-consistent solution of Schrödinger and Poisson equations (Hartree approximation), the dashed-dotted curve shows the exchange correction $e_{12}-\Delta e_1^{\mathrm{exch}}$, the dashed curve represents the depolarization shift $e_{12}\sqrt{1+\alpha}$, the dotted curves shows the excitonic shift $e_{12}\sqrt{1-\beta}$, and the full curve with black circles presents the ISB absorption energy after applying all the abovementioned corrections. As expected, when accounting only for the screening of the internal field, the ISB energy decreases with carrier concentration. However, when including the many-body corrections, the opposite behavior is predicted and the ISB energy increases rapidly with carrier concentration. For an electron density of 5×10^{12} cm^{-2} the calculation predicts a blueshift of 60 meV with respect to the unpopulated QW. The major contribution to the blueshift is due to the exchange interaction.[49]

We now focus on the calculation of the interband photoluminescence energy. In order to get insight in the valence band, one may use the approach of Suzuki and Uenoyama which is based on an eight-band $\mathbf{k}\cdot\mathbf{p}$ treatment of wurtzite GaN/AlGaN QWs in the presence of strain.[44] However, the accuracy of the hole confinement energy suffers from the present uncertainty in the values of the Luttinger parameters of nitrides. Since the interband luminescence only involves heavy holes from the upper A band of GaN, an entire description of the valence band dispersion is not necessary. In the following, we use an effective mass model to estimate the hole confinement energy. We consider that the A band exhibits almost a parabolic dispersion at the Γ point, and the effective mass for the heavy hole is taken as $m_{hh}=1.1m_0$.[45]

In terms of the strain-dependent energy gap of GaN, we assume that the strain state in the MQWs is the same as in the cap layer and we take the GaN gap energy equal to the experimental value of the PL energy of the GaN cap layer (3.46–3.48 eV). In addition, we do not correct the PL energies for the excitonic binding energy both for bulk GaN and the QWs, which is justified considering the uncertainty attached to the exact value of the heavy hole effective mass. Finally, we use the potential profile of an empty valence band for undoped samples and the potential profile deduced from the self-consistent treatment for electrons for doped samples.

It is well known that the PL energy for thick QWs strongly depends on the internal electric field and thus on the polarization discontinuity at the GaN-AlN interface. Taking the same value for static dielectric constant $\epsilon_r=10.4$ (Ref. 46) for both materials, and using the parameters proposed in Refs. 47 and 48, the polarization discontinuity at the GaN-AlN interface can be estimated as $\frac{\Delta P}{\epsilon_0 \epsilon_r}=9.2-9.7$ MV/cm assuming the in-plane lattice parameter of AlN or as 11.1–12.4 MV/cm assuming the in-plane lattice parameter of GaN. Because of the dispersion in $\frac{\Delta P}{\epsilon_0 \epsilon_r}$ value, we have introduced the polarization discontinuity as an adjustable parameter.

IV. COMPARISON WITH EXPERIMENTAL DATA

In this section, we compare the experimental energies of the PL and ISB absorption with the theoretical predictions. The calculated PL energy as a function of QW thickness is plotted in Figs. 10(a) and 10(b) for $\frac{\Delta P}{\epsilon_0 \epsilon_r}$ equal to 8 MV/cm

(dotted curve), 10 MV/cm (full curve) and 12 MV/cm (dashed curve). Figure 10(a) corresponds to UD samples and Fig. 10(b)—to samples doped with an electron concentration of 5×10^{19} cm^{-3} in the QWs. The open squares show the measurements. We assume the thickness deduced from the ISB measurements with 1 ML fluctuation. The best fit of the measured PL energies is obtained for $\frac{\Delta P}{\epsilon_0\epsilon_r}$ equal to 10 ± 1 MV/cm, in good agreement with previous estimations.[16]

We fix $\frac{\Delta P}{\epsilon_0\epsilon_r}$ equal to 10 MV/cm for further simulations of the ISB transition energy. Figure 11 shows the calculated e_{12} and e_{13} transition energies as a function of the QW thickness for samples doped in QWs at 5×10^{19} cm^{-3}. The barrier thickness is 3 nm. The CB offset at the GaN-AlN interface is taken as an adjustable parameter. In Fig. 11, the value of the CB offset is 1.95 eV (dashed curves), 1.85 eV (dotted curves), 1.75 eV (full curves) and 1.65 (dashed-dotted curves), respectively. The full circles show the experimental data. For samples with structured absorption spectrum all the peaks are plotted. We also assume a well thickness corresponding to an integer number of MLs as explained in Sec. II C.

For thick QWs, where more than two bound states are present, the observed e_{13} transition energy is reported in Fig. 11. However, since the e_{13} absorption is weak and strongly broadened, the peak energy is determined with an uncertainty as shown by the vertical error bars in Fig. 11. The horizontal bars stand for the uncertainty of the exact thickness giving rise to the e_{13} absorption.

As expected, the value of the CB offset has a strong influence on the e_{12} ISB energy for thin QWs because the excited state lies close in energy to the barrier CB. The best fit to the experimental values is obtained for a CB offset between 1.65 and 1.75 eV. From the excellent agreement with the experiments, we can conclude that the CB offset is smaller than the initially suggested value of 2 eV.[3,6,20]

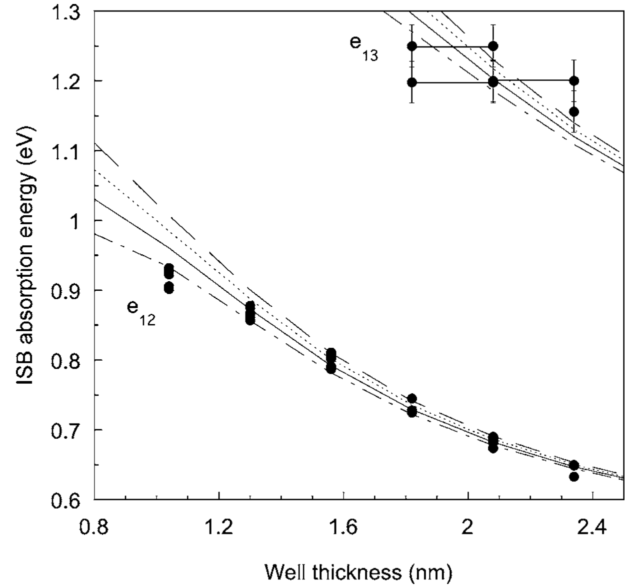

FIG. 11. Calculated e_{12} and e_{13} transition energies as a function of the QW width for samples doped in the QWs at 5×10^{19} cm^{-3}. Four CB offsets are used: 1.95 eV (dashed lines), 1.85 eV (dotted lines), 1.75 eV (full lines), and 1.65 (dashed-dotted lines). The full circles represent experimental data.

V. CONCLUSIONS

In conclusion, we have performed a systematic study of electron confinement in wurtzite phase GaN/AlN QWs with well thickness varying between 1 and 2.5 nm. Strong ISB absorptions covering the 1.33–1.91 μm range have been measured. The absorption line shape exhibits either a pure Lorentzian shape or multiple peaks. In the first case the broadening is homogeneous with a state-of-the-art low value of 67 meV. We deduce a dephasing time of the electrons in the excited subband T_2 of about 20 fs. For structured spectra the absorption can be perfectly reproduced with a sum of several Lorentzian curves; the individual peaks originate from absorption in QW regions with thickness equal to an integer number of monolayers.

We have also carried out simulations of the electronic structure which point out the relevance of the nonparabolicity and many-body corrections on the ISB absorption energy. The energy difference between parabolic and nonparabolic cases can be as large as 25%. We have also shown that, despite the internal field screening, the ISB absorption is blueshifted with doping because of many-body effects dominated by the exchange interaction. An excellent agreement with the experimental data is demonstrated. The best fit is achieved using a conduction band offset at the GaN/AlN heterointerfaces of 1.7 ± 0.05 eV and a polarization discontinuity $\frac{\Delta P}{\epsilon_0\epsilon_r}$ of 10 ± 1 MV/cm.

ACKNOWLEDGMENTS

The authors would like to acknowledge Le Si Dang, B. Daudin, and A. Lusson for fruitful collaboration. Part of the transmission electron microscopy measurements were carried out in the Central Facility of High Resolution Electron Microscopy of Friedrich-Alexander University Erlangen-Nürnberg, Germany. The authors would like to acknowledge the financial support of the 6th European Framework Programme within the STREP project NITWAVE (Contract No. 004170).

*Electronic address: maria.tchernycheva@ief.u-psud.fr

[1] S. Nakamura, M. Senoh, S. Nagahama, N. Iwasa, T. Yamada, T. Matsushita, H. Kiyoku, and Y. Sugimoto, Jpn. J. Appl. Phys., Suppl. **35**, L74 (1996).
[2] I. Akasaki, S. Sota, H. Sakai, T. Tanaka, M. Koike, and H. Amano, Electron. Lett. **32**, 1105 (1996).
[3] N. Suzuki and N. Iizuka, Jpn. J. Appl. Phys., Suppl. **36**, L1006 (1997).
[4] C. Gmachl, H. M. Ng, S. N. G. Chu, and A. Y. Cho, Appl. Phys. Lett. **77**, 3722 (2000).
[5] C. Gmachl, H. M. Ng, and A. Y. Cho, Appl. Phys. Lett. **79**, 1590 (2001).
[6] K. Kishino, A. Kikuchi, H. Kanazava, and T. Tachibana, Appl. Phys. Lett. **81**, 1234 (2002).
[7] A. Helman, M. Tchernycheva, A. Lusson, E. Warde, F. H. Julien, Kh. Moumanis, G. Fishman, E. Monroy, B. Daudin, D. Le Si Dang, E. Bellet-Amalric, and D. Jalabert, Appl. Phys. Lett. **83**, 5196 (2003).
[8] N. Suzuki and N. Iizuka, Jpn. J. Appl. Phys., Suppl. **38**, L363 (1999).
[9] S. Nicolay, J. F. Carlin, E. Feltin, R. Butte, M. Mosca, N. Grandjean, M. Ilegems, M. Tchernycheva, L. Nevou, and F. H. Julien, Appl. Phys. Lett. **87**, 111106 (2005).
[10] K. Moumanis, A. Helman, F. Fossard, M. Tchernycheva, A. Lusson, F. H. Julien, B. Damilano, N. Grandjean, and J. Massies, Appl. Phys. Lett. **82**, 868 (2003).
[11] M. Tchernycheva, L. Nevou, L. Doyennette, A. Helman, R. Colombelli, F. H. Julien, F. Guillot, E. Monroy, T. Shibata, and M. Tanaka, Appl. Phys. Lett. **87**, 101912 (2005).
[12] N. Iizuka, K. Kaneko, and N. Suzuki, Appl. Phys. Lett. **81**, 1803 (2002).
[13] J. Heber, C. Gmachl, H. Ng, and A. Cho, Appl. Phys. Lett. **81**, 1237 (2002).
[14] J. Hamazaki, S. Matsui, H. Kunugita, K. Ema, H. Kanazawa, T. Tachibana, A. Kikuchi, and K. Kishino, Appl. Phys. Lett. **84**, 1102 (2004).
[15] F. Bernardini, V. Fiorentini, and D. Vanderbilt, Appl. Phys. Lett. **56**, R10024 (1997).
[16] C. Adelmann, E. Sarigiannidou, D. Jalabert, Y. Hori, J.-L. Rouvière, B. Daudin, S. Danget, C. Bru-Chevallier, T. Shibata, and M. Tanaka, Appl. Phys. Lett. **82**, 4154 (2003).
[17] M. Helm, in *Intersubband Transitions in Quantum Wells: Physics and Device Applications II, Semiconductors and Semimetals Vol. 62*, edited by H. C. Liu and F. Capasso (Academic Press, San Diego, 2000), Vol. 62.
[18] K. Hoshino, T. Someya, K. Hirakawa, and Y. Arakawa, Phys. Status Solidi A **192**, 27 (2003).
[19] N. Suzuki, N. Iizuka, and K. Kaneko, Jpn. J. Appl. Phys., Suppl. **42**, 132 (2003).
[20] H. M. Ng, C. Gmachl, S. N. G. Chu, and A. Y. Cho, J. Cryst. Growth **220**, 432 (2000).
[21] J. R. Waldrop and R. W. Grant, Appl. Phys. Lett. **68**, 2879 (1996).
[22] A. Rizzi, R. Lantier, F. Monti, H. Lüth, F. D. Sala, A. D. Carlo, and P. Lugli, J. Vac. Sci. Technol. A **17**, 1674 (1999).
[23] E. Sarigiannidou, E. Monroy, N. Gogneau, G. Radtke, P. Bayle-Guillemaud, E. Bellet-Amalric, B. Daudin, and J. Rouvière, Semicond. Sci. Technol. (to be published).
[24] E. Monroy, B. Daudin, E. Bellet-Amalric, N. Gogneau, D. Jalabert, F. Enjalbert, J. Brault, J. Barjon, and L. S. Dang, J. Appl. Phys. **93**, 1550 (2003).
[25] N. Gogneau, G. Jalabert, E. Monroy, E. Sarigiannidou, J.-L. Rouvière, T. Shibata, M. Tanaka, J.-M. Gérard, and B. Daudin, J. Appl. Phys. **96**, 1104 (2004).
[26] D. Bowen and B. Tanner, *High Resolution Diffractometer and Topography* (Taylor and Francis Ltd., New York, 1998).
[27] L. C. West and S. J. Eglash, Appl. Phys. Lett. **46**, 1156 (1985).
[28] J. P. Ibbetson, P. T. Fini, K. D. Ness, S. P. DenBaars, J. S. Speck, and U. K. Mishra, Appl. Phys. Lett. **77**, 250 (2000).
[29] G. A. Slack, L. J. Schowalter, D. Morelli, and J. J. A. Freitas, J. Cryst. Growth **246**, 287 (2002).
[30] N. W. Ashcroft and N. D. Mermin, *Solid State Physics* (Holt, Rinehart and Winston, New York, 1976).
[31] F. Bernardini and V. Fiorentini, Phys. Rev. B **57**, R9427 (1998).
[32] M. Leroux, N. Grandjean, M. Laugt, J. Massies, B. Gil, P. Lefebvre, and P. Bigenwald, Phys. Rev. B **58**, R13371 (1998).
[33] J.-G. S. Demers and R. Maciejko, J. Appl. Phys. **90**, 6120 (2001).
[34] S. L. Chuang and C. S. Chang, Phys. Rev. B **54**, 2491 (1996).
[35] I. Vurgaftman, J. R. Meyer, and L. R. Ram-Mohan, J. Appl. Phys. **89**, 5815 (2001).
[36] G. Bastard, *Wave Mechanics Applied to Semiconductor Heterostructures* (Les Editions de Physique, Les Ulis, France, 1988).
[37] M. Tchernycheva, A. Helman, E. Warde, A. Lusson, and F. H. Julien, in *Proceedings of the International Conference on Information and Communication Technologies: from Theory to Applications* (IEEE, Piscataway, NJ, 2004), p. 179.
[38] V. Fock, Z. Phys. **61**, 126 (1930).
[39] Marie S.-C. Luo, S. L. Chuang, S. Schmitt-Rink, and A. Pinczuk, Phys. Rev. B **48**, 11 086 (1993).
[40] K. M. S. V. Bandara, D. D. Coon, O. Byungsung, Y. F. Lin, and M. H. Francombe, Appl. Phys. Lett. **53**, 1931 (1988); **55**, 206(E) (1989) for the correct value of the numerical coefficient.
[41] S. J. Allen, D. C. T. Jr, and B. Vinter, Solid State Commun. **20**, 425 (1976).
[42] T. Ando, Solid State Commun. **21**, 133 (1977).
[43] W. L. Bloss, J. Appl. Phys. **66**, 3639 (1989).
[44] M. Suzuki and T. Uenoyama, in *Group III Nitride Semiconductor Compounds*, edited by B. Gil (Oxford University Press, Oxford, 1998).
[45] S. Kalliakos, P. Lefebvre, and T. Taliercio, Phys. Rev. B **67**, 205307 (2003).
[46] A. S. Barker and M. Ilegems, Phys. Rev. B **7**, 743 (1973).
[47] O. Ambacher, J. Smart, J. R. Shealy, N. G. Weimann, K. Chu, M. Murphy, W. J. Schaff, L. F. Eastman, R. Dimitrov, L. Wittmer, M. Stutzmann, W. Rieger, and J. Hilsenbeck, J. Appl. Phys. **85**, 3222 (1999).
[48] V. Fiorentini, F. Bernardini, and O. Ambacher, Appl. Phys. Lett. **80**, 1204 (2002).
[49] Treating many-body effects, we have neglected the slight nonorthogonality of the envelope functions that arises from the energy dependence of the effective mass. However, we have found that the relative many-body correction in the parabolic and nonparabolic cases differs less than by 3% of its value therefore the nonorthogonality can be neglected.